PCCP

ROYAL SOCIETY OF CHEMISTRY

PAPER

View Article Online
View Journal | View Issue



Cite this: *Phys. Chem. Chem. Phys.*, 2024, **26**, 8681

# Double pyramid stacked CoO nano-crystals induced by graphene at low temperatures as highly efficient Fenton-like catalysts†

Kui Lu,‡[ab] Tao Ding,‡[a] Mengxiang Zhu,[a] Junjie Chen,[a] Dongting Yue,[a] Xing Liu,[a] Xiaoqin Fang,[b] Junfang Xia,[b] Zhiyuan Qin,[b] Minghong Wu*[a] and Guosheng Shi*[a]

Received 24th January 2024,
Accepted 21st February 2024

DOI: 10.1039/d4cp00334a

rsc.li/pccp



Transition metal oxides are widely used as Fenton-like catalysts in the treatment of organic pollutants, but their synthesis usually requires a high temperature. Herein, an all-solid-state synthesis method controlled by graphene was used to prepare a double pyramid stacked CoO nano-crystal at a low temperature. The preparation temperature decreased by 200 °C (over 30% reduction) due to the introduction of graphene, largely reducing the reaction energy barrier. Interestingly, the corresponding degradation rate constants ($k_{obs}$) of this graphene-supported pyramid CoO nano-crystals for organic molecules after their adsorption were over 2.5 and 35 times higher than that before adsorption and that of free CoO, respectively. This high catalytic efficiency is attributed to the adsorption of pollutants at the surface by supporting graphene layers, while free radicals activated by CoO can directly and rapidly contact and degrade them. These findings provide a new strategy to prepare low carbon-consuming transition metal oxides for highly efficient Fenton-like catalysts.

## 1. Introduction

Developing effective catalysts to replace precious metals has attracted widespread attention. Transition metals possess unoccupied valence d orbitals and numerous single electrons,[1–6] which facilitate the formation of steadfast metal ions or complexes, making them an ideal alternative to precious metal-based catalysts.[7–11] With the increasing population and the development of industrialization, persistent organic pollutants such as antibiotics and cyclic aromatic compounds have been detected in water samples from a wide range of living environments, and many efforts have been made to tackle this problem.[10,12–18] As an advanced oxidation technology, Fenton and Fenton-like processes employing transition metal oxide-based catalysts to address the continuous worsening of environmental pollution present promising potential for the development of various low-carbon and sustainable industrial production methods.[19–28]

However, in these catalytic processes, the related radicals have only a very limited lifetime. For example, the free radical half-lives of $^{\bullet}OH$ and $^{\bullet}SO_4^-$ are only 1 μs and 30–40 μs, respectively.[29–31] This leads to insufficient time for free radicals in the solution to diffuse to organic pollutants in the solution, thus seriously affecting degradation efficiency. New strategies to produce transition metal oxides with low-energy technologies and to minimise exposure to impurities and free radicals remain highly desirable.

In this study, CoO nano-crystals supported on graphene, named CoO@graphene, were successfully synthesized at a lower temperature. The treated temperature decreased from 600 °C down to only 400 °C due to the introduction of graphene, which largely reduces the reaction energy barrier for phase conversion. Interestingly, its corresponding degradation rate constants ($k_{obs}$) for organic molecules with pre-adsorption by graphene are over 2.5 and 35 times higher than that of CoO@graphene and CoO without pre-adsorption, respectively. Supporting graphene layers adsorb pollutants on the surface, while free radicals activated by CoO can directly and rapidly contact and degrade them.

## 2. Experimental

### 2.1 Chemicals and materials

Graphene (purchased from Wuxi Huxin Testing Technology Co., Ltd), cobalt chloride hexahydrate ($CoCl_2{\cdot}6H_2O$), peroxymonosulfate

[a] *Shanghai Applied Radiation Institute, State Key Lab. Advanced Special Steel, Shanghai University, Shanghai 200444, P. R. China. E-mail: gsshi@shu.edu.cn*
[b] *Shanghai Jingyu Environmental Engineering Co. Ltd., Xiner Road, Shanghai 200439, P. R. China*

† Electronic supplementary information (ESI) available. See DOI: https://doi.org/10.1039/d4cp00334a

‡ Kui Lu and Tao Ding have contributed equally.

(PMS), sodium hydroxide (NaOH, ≥96.0%), sulfuric acid ($H_2SO_4$, ≥98.0%), rhodamine B (RhB, $C_{28}H_{31}ClN_2O_3$, ≥99.0 wt%), benzoquinone (BQ), furfuryl alcohol (FFA), dimethyl sulfoxide (DMSO) acetone, methanol (MeOH), 5,5-dimethyl-1-pyrroline *N*-oxide (DMPO) and 2,2,6,6-tetramethyl-4-piperidinyloxyl (TEMP). Acetonitrile ($C_2H_3N$, ≥99.0 wt%), methyl phenyl sulfoxide (PMSO), methyl phenyl sulfone ($PMSO_2$), sodium chloride (NaCl), sodium sulfate ($Na_2SO_4$) and sodium carbonate ($Na_2CO_3$). The aqueous solutions of all the above reagents were prepared with deionized water and distilled water.

### 2.2 Synthesis of CoO@graphene

Precisely, 10 mg of graphene powder and cobalt chloride hexahydrate were mixed in a mortar, and after the powdered mixture was completely ground, it was transferred to a crucible and calcined in a tube furnace at 100 °C, 200 °C and 400 °C for 1 hour each. The argon gas flow rate was 150 mL $min^{-1}$, and the heating rate was 10 °C $min^{-1}$.

### 2.3 Synthesis of CoO

10 mg of cobalt chloride hexahydrate was accurately weighed and thoroughly ground in a mortar. The powder was then transferred to a crucible and calcined in a tubular furnace at 600 °C for 1 hour. An argon gas flow rate of 150 mL $min^{-1}$ and a heating rate of 10 °C $min^{-1}$ were maintained.

### 2.4 Radical quenching experiments

The use of the radical quenching experiment is a prevalent means for identifying active substances in AOPs. It is both intuitive and operable, whereby the intended active substance is completely suppressed with an excessive quenching agent, such as methanol ($CH_3OH$/TBA). Consequently, the production and contribution of reactive substances can be evaluated by observing the influence of adding or not adding the quenching agent on the organic dye's degradation efficiency. Abbreviations of technical terms are explained upon their initial introduction to avoid confusion. 10 mg of the catalyst and 20 mL of RhB solution with a quencher (TBA/MeOH = 100 mM, FFA = 1 mm, BQ = 10 mm) were combined in a glass beaker and stirred mechanically. Afterward, 90 ppm of PMS was added to initiate the Fenton-like reaction. A 1 mL suspension was collected at specified intervals and promptly centrifuged at 6000 rpm for 5 minutes to eliminate the catalyst. Methyl phenyl sulfoxide (PMSO, 100 μM), and methyl phenyl sulfone ($PMSO_2$, 100 μM), 10 mg catalyst (0.5 g $L^{-1}$), and 20 mL RhB solution (10 mg $L^{-1}$) were mixed in a glass beaker and mechanically stirred through the whole experiment process.

### 2.5 Material characterization

The crystal structure of the synthesized samples was determined using X-ray powder diffraction (XRD) on a Smartlab instrument (Rigaku D/max-2500) with Cu Kα radiation ($\lambda$ = 0.15405 nm). Sequential scans were conducted from 5° to 90° at a scanning rate of 20° $min^{-1}$. The field emission scanning electron microscopy (SEM, Gemini G300) was employed to characterize the morphologies. The surface properties were characterized by X-ray photoelectron spectroscopy (XPS, Thermo Scientific K-Alpha). The absorbance of the RhB solution was measured on an ultraviolet spectrophotometer (UV-1600). Electron paramagnetic resonance (EPR) spectra obtained using a JEOL FA200 were used to study the reactive radicals produced during PMS activation. These radicals were trapped by spin-trapping agents such as 5,5-dimethylpyrroline oxide (DMPO) and 2,2,6,6-tetramethyl-4-piperidinyloxyl (TEMP). High-performance liquid chromatography (HPLC, Thermo U3000) was used to determine the PMSO and $PMSO_2$ concentrations at fixed intervals during the decomposition process.

## 3. Results and discussion

Considering the cation–π interactions between metal cations and graphene,[15,35] CoO nano-crystals were prepared using an all-solid-state synthesis method controlled by graphene. The CoO nano-crystals supported by graphene, called CoO@graphene, were prepared by a thermal decomposition reaction of $CoCl_2{\cdot}6H_2O$ on graphene at a relatively low temperature. The catalytic process is illustrated in Fig. 1a. Graphene was prepared *via* vapor deposition. Then, 10 mg of graphene and 10 mg of $CoCl_2{\cdot}6H_2O$ were thoroughly mixed by grinding in a mortar. The resulting mixture was placed into a tube furnace and calcined at different temperatures (100, 200, 400 and 600 °C) for 60 minutes under an argon gas atmosphere. CoO was obtained at 400 °C in the presence of graphene, as displayed in Fig. 1b. In contrast, the CoO was obtained at 600 °C without graphene (Fig. 1b). The preparation temperature decreased by 200 °C (over 30% reduction), which can be ascribed to the introduction of graphene, largely reducing the reaction energy barrier for the phase conversion from the Co-based on the corresponding chloride salts.[32–34]

Using field emission scanning electron microscopy (FESEM), the crystal morphology of CoO@graphene was observed.

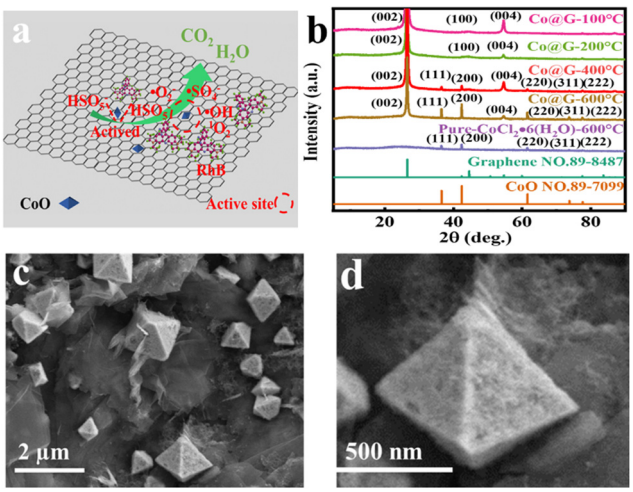


Fig. 1 (a) Schematic illustration of the Fenton-like catalysis mechanism *via* CoO@graphene. (b) X-ray diffraction (XRD) patterns of CoO@graphene and $CoCl_2{\cdot}6H_2O$ after calcination at various temperatures up to 600 °C. (c) and (d) The scanning electron microscopy (SEM) image of CoO@graphene and the size of single CoO.

Interestingly, we found many double pyramidal stacked CoO nano-crystals on the graphene surface (Fig. 1c). The elemental mapping analysis showed the uniform distribution of C, O and Co. The atom ratio of C, O and Co was 19 : 2.8 : 1 (Fig. S1, ESI†). The side length of the crystal is approximately 500 nm (Fig. 1d). The triangular surface of the crystal appeared frosted (Fig. 1c).

Such CoO@graphene nano-crystals showed high catalytic efficiency of the Fenton-like reaction. The sample was additionally washed and dried to remove unreacted soluble $CoCl_2 \cdot 6H_2O$ before use. 10 mg CoO@graphene nano-crystals were introduced into a 20 mL solution of rhodamine B (RhB) as an example of the organic pollutants at a concentration of 10 mg $L^{-1}$, followed by the initiation of the adsorption process in a 50 mL reactor for a duration of 2 hours. Then, 1 mL solution was withdrawn from the solution at time intervals of 0, 30, 60, 90 and 120 minutes to test the adsorption amount of RhB on the sample. The absorbance of the extracted solution was quantified using UV-visible absorption spectrometry. Finally, after 120 minutes of the adsorption process, a 100 μL solution of peroxymonosulfate (PMS) (18 g $L^{-1}$) was introduced to initiate the Fenton-like catalytic reaction. In only 5 minutes, the RhB degradation efficiency reached 100% (Fig. 2a). For comparison, controlled experiments of pure CoO and graphene at the same operating processes were performed. After 5 minutes, the RhB degradation efficiency reached only 12% and 67% for pure CoO and graphene, respectively (Fig. 2a).

To illustrate the influence of adsorption on the catalytic efficiency of CoO@graphene nano-crystals on organic pollutants, we performed the RhB degradation experiment without the organic pollutant adsorption process. A 100 μL solution of PMS (18 g $L^{-1}$) was directly introduced to the mixture solution of RhB and CoO@graphene nano-crystals without the 120-minute adsorption process to initiate the Fenton-like catalytic reaction. After 5 minutes, the RhB degradation efficiency reached only 83% (Fig. 2b). The CoO@graphene nano-crystals clearly showed a higher catalytic efficiency of the Fenton-like reaction after adsorption of the organic pollutants. To quantitatively evaluate the increment of the reaction efficiency, the corresponding pseudo-first-order degradation rate constants ($k_{obs}$) were calculated. Fig. 2c shows that the values of $k_{obs}$ for CoO@graphene with the adsorption treatment, without the adsorption treatment, and CoO were 0.770, 0.305 and 0.021 $min^{-1}$, respectively. Its corresponding $k_{obs}$ values for the former were more than 2.5 and 35 times higher than those for the latter two, respectively. We considered that the CoO can be produced on the graphene due to the cation–π interaction between $Co^{2+}$ and graphene flake. Besides, the contaminants and active species were also adsorbed on the CoO@graphene, overcoming the problem of the low utilization rate of active species because of their short half-lives. The high electron transport capacity of graphene accelerated the reaction process and improved the catalytic activity. In addition, we noted that the $k_{obs}$ value was also (6.6/60) times that of the CoO from other studies.[1]

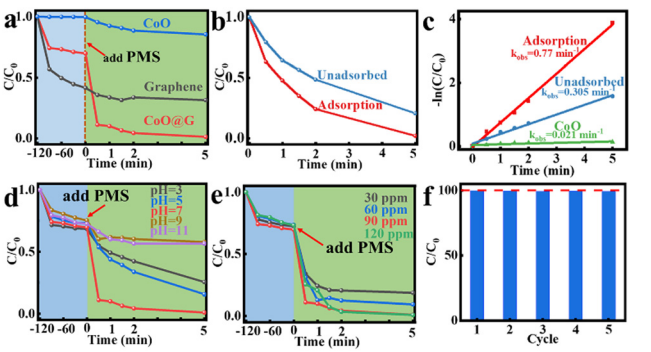


Fig. 2 (a) TRhB degradation was catalyzed by CoO@graphene calcined at 400 °C, graphene and pure CoO. (b) and (c) Different degradation efficiencies and corresponding degradation rate constants ($k_{obs}$) for CoO@graphene catalysts with or without adsorption treatment. (d) and (e) The degradation performance at different conditions. Reaction condition: solution pH = 3, 5, 7, 9 and 11; PMS = 30 ppm, 60 ppm, 90 ppm and 120 ppm. (f) The reusability of CoO@graphene catalysis.

CoO@graphene showed an exceptional degradation capacity within a wide pH range of 3 to 7. We performed the degradation experiments at different pH values from 3 to 11. Fig. 2d shows that the RhB degradation efficiency reached about 80% even if the pH value was reduced to 3, while it sharply decreased to only about 40% when the pH value increased to 9. It illustrated that the CoO@graphene showed a high degradation capacity under acid and neutral solutions. Furthermore, we also performed the influence of the dosages of the PMS added in the solution. Fig. 2e shows that the addition of PMS at 90 ppm completely degrades RhB.

Fig. 2f shows that the Fenton-like activity remained consistently high over the course of 5 cycles in the CoO@graphene/PMS system. In addition, the Fenton-like performance of the CoO@graphene/PMS system was also studied in the presence of 0.1 M NaCl, $Na_2SO_4$ and $Na_2CO_3$. As shown in Fig. S2 (ESI†), the degradation efficiency of Rhb in the presence of NaCl, $Na_2SO_4$ and $Na_2CO_3$ was higher than 98.0% within 5 min, indicating that the CoO@graphene/PMS system provides an effective way for saline organic wastewater treatment. Using X-ray photoelectron spectroscopy (XPS), we characterized the influence of Co in CoO@graphene before and after catalytic reactions. From a full-scale XPS survey of CoO@graphene, we observed the presence of C, Co and O elements (Fig. S3, ESI†). We also measured the changes in the chemical states of the Co elements on the surface of CoO@graphene. Fig. 3b shows the XPS spectrum of the CoO@graphene with the peaks of binding energies at 781.09 eV and 783.77 eV, evidencing the presence of Co(II); meanwhile, the two peaks at 797.78 eV and 796.46 eV correspond to Co(III).[36,37] We found, after the Fenton-like reaction, the mole ratio of Co(II) slightly decreased from 54.7% to 53.9%, and the corresponding amount of Co(III) slightly increased from 19.8% to 20.5%. This illustrated that the Co was stable in the catalytic process, indicating that CoO@graphene has a good catalytic cycle stability,[9,38] which further confirmed the cycle catalytic experimental results.

To illustrate the molecular mechanism of the CoO@graphene/PMS catalytic system, we investigated the possible reactive species such as $^{\bullet}OH$, $^{\bullet}SO_4^-$, $^{\bullet}O_2^-$ and $^1O_2$ by the free radical quenching

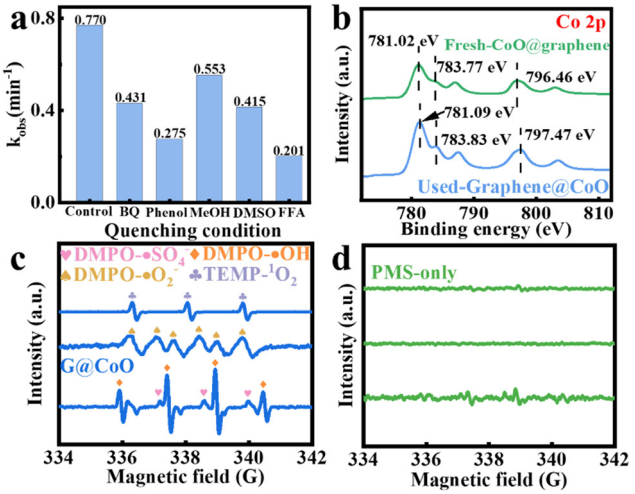


Fig. 3 (a) Pseudo-first order rate constants ($k_{obs}$) from quenching experiments. (b) High resolution spectra of Co 2p for fresh and used CoO@graphene. (c) and (d) EPR spectra of DMPO and TEMP adducts for CoO@graphene/PMS and pure PMS reaction systems.

experiments. Fig. 3a shows that the Fenton-like catalytic rate coefficients of methanol for $^{\bullet}OH$ together with the $^{\bullet}SO_4^-$ scavenger and phenol for the $^{\bullet}OH$ scavenger in the CoO@graphene/PMS system was reduced from 0.770 $min^{-1}$ to 0.553 $min^{-1}$ and 0.275 $min^{-1}$, respectively. This indicated the presence of $^{\bullet}OH$. Furthermore, the reaction rate $k_{obs}$ decreased from 0.770 to 0.431 $min^{-1}$, when benzoquinone (BQ) for $^{\bullet}O_2^-$ inhibitor was incorporated. It indicated an important role of $^{\bullet}O_2^-$ in the Fenton-like systems. Finally, the addition of furfuryl alcohol (FFA) significantly decreased the catalytic efficiency of RhB, and the value of $k_{obs}$ was reduced from 0.770 to 0.201 $min^{-1}$. This demonstrates that $^1O_2$ plays a dominant role in this Fenton-catalyzed RhB degradation reaction.

To further verify the active species in the Fenton-like reaction, the trapped electron paramagnetic resonance (EPR) of 5,5-dimethylpyrroline-oxide (DMPO) experiments were conducted. Fig. 3d shows that no characteristic signals were detected when PMS was added to the reaction system, indicating that PMS hardly generates radicals without the activation of catalysts. However, when the CoO@graphene sample was added into the system, the characteristic signals for $^{\bullet}SO_4^-$ $^{\bullet}OH$ and $^{\bullet}O_2^-$ were detected, demonstrating that PMS can produce $^{\bullet}SO_4^-$ and $^{\bullet}OH$ by the activation of the catalysts. The quantitative information of 2,2,6,6-tetramethyl-4-piperidinyloxyl (TEMPX) adducts, resulting from the reaction between $^1O_2$ and TEMP, can be observed. Double electron transfer was shown to form Co(IV) in cobalt-based catalysts/peroxides. The RhB degradation decreased significantly in the presence of DMSO associated with the decrease of $k_{obs}$ from 0.770 to 0.415 $min^{-1}$ (Fig. 3a). The conversion efficiency from PMSO to $PMSO_2$ was 85.7% (Fig. S4, ESI†). These results suggested that Co(IV) was an important active species in the CoO@graphene/PMS system. Oxidation of micropollutants is typically dominated by peroxides, such as PMS and peracetic acid. The oxidation of micropollutants is typically dominated by peroxides such as PMS and peracetic acid in cobalt-based catalysts/peroxides.

Thus, we can describe the possible mechanism process for the CoO@graphene/PMS system[39–44] using the following equations:

$$Co^{2+} + HSO_5^- = Co^{3+} + {}^{\bullet}SO_4^- + OH^-$$

$$^{\bullet}SO_4^- + H_2O = SO_4^{2-} + {}^{\bullet}OH + H^+$$

$$^{\bullet}SO_4^- + OH^- = SO_4^{2-} + {}^{\bullet}OH$$

$$Co^{3+} + HSO_5^- = Co^{2+} + {}^{\bullet}SO_5^- + H^+$$

The Co species can activate PMS to generate hydroxyl radicals and sulfate radicals. Part of the $^{\bullet}SO_4^-$ produced will react with water in the solution to form $^{\bullet}OH$, while the remainder will be adsorbed onto the graphene surface to occupy the active site. The hydration of $SO_5^{2-}$ to form $H_2O_2$, which is then regenerated to form $^{\bullet}O_2^-$, can be described as the mechanism for the production of $^{\bullet}O_2^-$. The generation of $^1O_2$ was not only attributed to the autoxidation of peroxymonosulfate (PMS) but also resulted from the chemical interaction between the superoxide anion radical ($^{\bullet}O_2^-$) and hydroxyl radical ($^{\bullet}OH$).[45,46] It can be described using the following equations:

$$SO_5^{2-} + H_2O = SO_4^{2-} + H_2O_2$$

$$^{\bullet}HO_2 = H^+ + {}^{\bullet}O_2^-$$

$$HSO_5^- = {}^{\bullet}SO_5^- + H^+ + e^-$$

$$2{}^{\bullet}SO_5^- = S_2O_8^{2-} + {}^1O_2$$

$$^{\bullet}OH + {}^{\bullet}O_2^- = OH^- + {}^1O_2$$

## 4. Conclusions

In summary, CoO@graphene with pyramid CoO nano-crystals was prepared using a facile calcination approach at a relatively lower temperature. The treatment temperature could be reduced by 200 °C (over 30% reduction) because of the introduction of graphene, largely reducing the reaction energy barrier. Interestingly, its corresponding degradation rate constants ($k_{obs}$) for organic molecules with pre-adsorption by graphene are over 2.5 and 35 times higher than those of CoO@graphene and CoO without pre-adsorption, respectively. It can be ascribed to the adsorption of the supporting graphene layers for pollutants, while the free radicals activated by the CoO can directly make rapid contact and degrade them. Our findings provide a viable strategy to prepare transition metal oxides with lower-carbon consumption and graphene-supporting transition metal oxides for highly efficient Fenton-like catalysts.

## Author contributions

Guosheng Shi and Minghong Wu designed the project. Kui Lu, Tao Ding, Mengxiang Zhu, Junjie Chen, Dongting Yue and Xing Liu performed the experiments. Kui Lu, Tao Ding, Xiaoqin

Fang, Junfang Xia, Zhiyuan Qin and Guosheng Shi analyzed the data and co-wrote the paper. All authors discussed the results and commented on the manuscript.

## Conflicts of interest

There are no conflicts to declare.

## Acknowledgements

This work was supported by the National Natural Science Foundation of China (U1932123, 12105166), the National Science Fund for Outstanding Young Scholars (No. 11722548).

## Notes and references

1 X. Li, X. Huang, S. Xi, S. Miao, J. Ding, W. Cai, S. Liu, X. Yang, H. Yang and J. Gao, *et al.*, Single Cobalt Atoms Anchored on Porous N-Doped Graphene with Dual Reaction Sites for Efficient Fenton-like Catalysis, *J. Am. Chem. Soc.*, 2018, **140**(39), 12469–12475.

2 M. Li, K. Zheng, Y. T. Jin, Z. X. Zhang, J. L. Cheng, L. W. Huang, C. H. Mo and S. Q. Zhou, Cobalt/nitrogen co-carved carbon nanorod for efficient Fenton-like reaction: Degradation efficacy, reaction mechanism and singlet oxygen generation, *J. Mater. Sci. Technol.*, 2023, **137**, 67–78.

3 J. V. Obligacion and P. J. Chirik, Earth-abundant transition metal catalysts for alkene hydrosilylation and hydroboration, *Nat. Rev. Chem.*, 2018, **2**(5), 15–34.

4 R. Yang, Y. Fan, Y. Zhang, L. Mei, R. Zhu, J. Qin, J. Hu, Z. Chen, Y. Hau Ng and D. Voiry, *et al.*, 2D Transition Metal Dichalcogenides for Photocatalysis, *Angew. Chem., Int. Ed.*, 2023, **62**, e20218016.

5 U. B. Kim, D. J. Jung, H. J. Jeon, K. Rathell and S. G. Lee, Synergistic Dual Transition Metal Catalysis, *Chem. Rev.*, 2020, **120**(24), 13382–13433.

6 P. S. Steinlandt, L. Zhang and E. Meggers, Metal Stereogenicity in Asymmetric Transition Metal Catalysis, *Chem. Rev.*, 2023, **123**(8), 4764–4794.

7 W. Shao, C. He, M. Zhou, C. Yang, Y. Gao, S. Li, L. Ma, L. Qiu, C. Cheng and C. Zhao, Core–shell-structured MOF-derived 2D hierarchical nanocatalysts with enhanced Fenton-like activities, *J. Mater. Chem. A*, 2020, **8**(6), 3168–3179.

8 X. Yu, L. Wang, X. Wang, H. Liu, Z. Wang, Y. Huang, G. Shan, W. Wang and L. Zhu, Enhanced nonradical catalytic oxidation by encapsulating cobalt into nitrogen doped graphene: highlight on interfacial interactions, *J. Mater. Chem. A*, 2021, **9**(11), 7198–7207.

9 H. Shi, Y. He, Y. Li and P. Luo, 2D MOF derived cobalt and nitrogen-doped ultrathin oxygen-rich carbon nanosheets for efficient Fenton-like catalysis: Tuning effect of oxygen functional groups in close vicinity to Co-N sites, *J. Hazard. Mater.*, 2023, **443**, 130345.

10 J. Hu, X. Zeng, G. Wang, B. Qian, Y. Liu, X. Hu, B. He, L. Zhang and X. Zhang, Modulating mesoporous $Co_3O_4$ hollow nanospheres with oxygen vacancies for highly efficient peroxymonosulfate activation, *Chem. Eng. J.*, 2020, **400**, 125869.

11 Z. Pei, H. Zhang, Y. Guo, D. Luan, X. Gu and X. W. Lou, Atomically Dispersed Fe Sites Regulated by Adjacent Single Co Atoms Anchored on N-P co-doped Carbon Structures for Highly Efficient Oxygen Reduction Reaction, *Adv. Mater.*, 2023, **30**, 2306047.

12 K. Yin, R. Wu, Y. Shang, D. Chen, Z. Wu, X. Wang, B. Gao and X. Xu, Microenvironment modulation of cobalt single-atom catalysts for boosting both radical oxidation and electron-transfer process in Fenton-like system, *Appl. Catal., B*, 2023, **329**, 122558.

13 X. Lu, J. Hou, K. Yang, L. Zhu, B. Xing and D. Lin, Binding Force and Site-Determined Desorption and Fragmentation of Antibiotic Resistance Genes from Metallic Nanomaterials, *Environ. Sci. Technol.*, 2021, **55**(13), 9305–9316.

14 H. Chen, X. Liu, D. Gong, C. Zhu, G. Liu, J. Fan, P. Wu, Z. Li, Y. Pan and G. Shi, *et al.*, Ultrahigh-water-flux desalination on graphdiyne membranes, *Nat. Water*, 2023, **1**(9), 800–807.

15 L. Chen, G. Shi, J. Shen, B. Peng, B. Zhang, Y. Wang, F. Bian, J. Wang, D. Li and Z. Qian, *et al.*, Ion sieving in graphene oxide membranes *via* cationic control of interlayer spacing, *Nature*, 2017, **550**(7676), 380–383.

16 J. Chen, X. Liu, Z. Ding, Z. He, H. Jiang, K. Zhu, Y. Li and G. Shi, Multistage Filtration Desalination *via* Ion Self-Rejection Effect in Cation-Controlled Graphene Oxide Membrane under 1 Bar Operating Pressure, *Nano Lett.*, 2023, **23**(23), 10884–10891.

17 D. Gong, X. Liu, P. Wu, Y. Wang, B. Guo, S. Liu, H. Chen, Y. Yin, G. Liu and M. Liu, *et al.*, Water pumping effect over the organic ions defined graphene oxide membrane impulses high flux desalination. npj Clean, *Water*, 2022, **5**(1), 68.

18 G. Shi, L. Chen, Y. Yang, D. Li, Z. Qian, S. Liang, L. Yan, L. H. Li, M. Wu and H. Fang, Two-dimensional Na–Cl crystals of unconventional stoichiometries on graphene surface from dilute solution at ambient conditions, *Nat. Chem.*, 2018, **10**(7), 776–779.

19 D. Fu, Y. Park and M. E. Davis, Confinement effects facilitate low-concentration carbon dioxide capture with zeolites, *Proc. Natl. Acad. Sci. U. S. A.*, 2022, **119**(39), e2211544119.

20 M. A. Shannon, P. W. Bohn, M. Elimelech, J. G. Georgiadis, B. J. Mariñas and A. M. Mayes, Science and technology for water purification in the coming decades, *Nature*, 2008, **452**(7185), 301–310.

21 B. C. Hodges, E. L. Cates and J. H. Kim, Challenges and prospects of advanced oxidation water treatment processes using catalytic nanomaterials, *Nat. Nanotechnol.*, 2018, **13**(8), 642–650.

22 Y. Shang, Y. Kan and X. Xu, Stability and regeneration of metal catalytic sites with different sizes in Fenton-like system, *Chin. Chem. Lett.*, 2023, **34**(8), 108278.

23 M. Huang, X. Wang, C. Liu, G. Fang, J. Gao, Y. Wang and D. Zhou, Facile ball milling preparation of sulfur-doped carbon as peroxymonosulfate activator for efficient removal of organic pollutants, *J. Environ. Chem. Eng.*, 2021, **9**(6), 106539.

24 S. Ma, D. Yang, Y. Guan, Y. Yang, Y. Zhu, Y. Zhang, J. Wu, L. Sheng, L. Liu and T. Yao, Maximally exploiting active sites on Yolk@shell nanoreactor: Nearly 100% PMS activation efficiency and outstanding performance over full pH range in Fenton-like reaction, *Appl. Catal., B*, 2022, **316**, 121594.
25 H. Bao, Y. Qiu, X. Peng, J. A. Wang, Y. Mi, S. Zhao, X. Liu, Y. Liu, R. Cao and L. Zhuo, *et al.*, Isolated copper single sites for high-performance electroreduction of carbon monoxide to multicarbon products, *Nat. Commun.*, 2021, **12**(1), 238.
26 J. Zhang, Y. Zhao, X. Guo, C. Chen, C. L. Dong, R. S. Liu, C. P. Han, Y. Li, Y. Gogotsi and G. Wang, Single platinum atoms immobilized on an MXene as an efficient catalyst for the hydrogen evolution reaction, *Nat. Catal.*, 2018, **1**(12), 985–992.
27 W. D. Oh, Z. Dong, G. Ronn and T. T. Lim, Surface–active bismuth ferrite as superior peroxymonosulfate activator for aqueous sulfamethoxazole removal: Performance, mechanism and quantification of sulfate radical, *J. Hazard. Mater.*, 2017, **325**, 71–81.
28 W. D. Oh, Z. Dong and T. T. Lim, Generation of sulfate radical through heterogeneous catalysis for organic contaminants removal: Current development, challenges and prospects, *Appl. Catal., B*, 2016, **194**, 169–201.
29 T. Olmez Hanci and I. Arslan-Alaton, Comparison of sulfate and hydroxyl radical based advanced oxidation of phenol, *Chem. Eng. J.*, 2013, **224**, 10–16.
30 P. Hu and M. Long, Cobalt-catalyzed sulfate radical-based advanced oxidation: A review on heterogeneous catalysts and applications, *Appl. Catal., B*, 2016, **181**, 103–117.
31 L. Wu, B. Li, Y. Li, X. Fan, F. Zhang, G. Zhang, Q. Xia and W. Peng, Preferential Growth of the Cobalt (200) Facet in Co@N–C for Enhanced Performance in a Fenton-like Reaction, *ACS Catal.*, 2021, **11**(9), 5532–5543.
32 L. Li, R. Huang, X. R. Cao and Y. H. Wen, Computational screening of efficient graphene-supported transition metal single atom catalysts toward the oxygen reduction reaction, *J. Mater. Chem. A*, 2020, **8**, 19319–19327.
33 X. Chen and R. Hu, DFT-based study of single transition metal atom doped g-$C_3N_4$ as alternative oxygen reduction reaction catalysts, *Int. J. Hydrogen Energy*, 2019, **44**, 15409–15416.
34 H. Fei, J. Dong, M. J. Arellano-Jiménez, G. Ye, N. Dong Kim, E. L. G. Samuel, Z. Peng, Z. Zhu, F. Qin, J. Bao, M. J. Yacaman, P. M. Ajayan, D. Chen and J. M. Tour, Atomic cobalt on nitrogen-doped graphene for hydrogen generation, *Nat. Commun.*, 2015, **6**, 8668.
35 H. Li, X. Liu, S. Qi, L. Xu, G. Shi, Y. Ding, X. Yan, Y. Huang and J. Geng, *Angew. Chem., Int. Ed.*, 2017, **56**, 14090–14095.
36 P. K. Klu, M. A. Nasir Khan, C. Wang, J. Qi, X. Sun and L. Jiansheng, Mechanism of peroxymonosulfate activation and the utilization efficiency using hollow (Co, Mn)$_3O_4$ nanoreactor as an efficient catalyst for degradation of organic pollutants, *Environ. Res.*, 2022, **207**, 112148.
37 C. Cai, S. Kang, X. Xie, C. Liao, X. Duan and D. D. Dionysiou, Efficient degradation of bisphenol A in water by heterogeneous activation of peroxymonosulfate using highly active cobalt ferrite nanoparticles, *J. Hazard. Mater.*, 2020, **399**, 122979.
38 Q. T. Sun, B. D. Xu, J. Yang, T. T. Qian and H. Jiang, Layered oxides supported Co-Fe bimetal catalyst for carbamazepine degradation *via* the catalytic activation of peroxymonosulfate, *Chem. Eng. J.*, 2020, **400**, 125899.
39 X. Zhang, X. Yan, X. Hu, R. Feng, M. Zhou and L. Wang, Efficient removal of organic pollutants by a Co/N/S-doped yolk–shell carbon catalyst via peroxymonosulfate activation, *J. Hazard. Mater.*, 2022, **421**, 126726.
40 J. Yang, D. Zeng, J. Li, L. Dong, W.-J. Ong and Y. He, A highly efficient Fenton-like catalyst based on isolated diatomic Fe-Co anchored on N-doped porous carbon, *Chem. Eng. J.*, 2021, **404**, 126376.
41 F. Yang, B. Wang, H. Su, S. Zhou and Y. Kong, Thermal-induced surface defective Co/Fe–Co planar hybrid composite nanosheet with enhanced catalytic activity in the Fenton-like reaction, *Mater. Chem. Front.*, 2017, **1**(10), 2065–2077.
42 G. X. Huang, C. Y. Wang, C. W. Yang, P. C. Guo and H. Q. Yu, Degradation of Bisphenol A by Peroxymonosulfate Catalytically Activated with $Mn_{1.8}Fe_{1.2}O_4$ Nanospheres: Synergism between Mn and Fe, *Environ. Sci. Technol.*, 2017, **51**(21), 12611–12618.
43 B. Zhang, X. Li, K. Akiyama, P. A. Bingham and S. Kubuki, Elucidating the Mechanistic Origin of a Spin State-Dependent FeNx–C Catalyst toward Organic Contaminant Oxidation *via* Peroxymonosulfate Activation, *Environ. Sci. Technol.*, 2021, **56**(2), 1321–1330.
44 Q. Yan, C. Lian, K. Huang, L. Liang, H. Yu, P. Yin, J. Zhang and M. Xing, Constructing an Acidic Microenvironment by MoS2 in Heterogeneous Fenton Reaction for Pollutant Control, *Angew. Chem., Int. Ed.*, 2021, **60**(31), 17155–17163.
45 X. Li, A. I. Rykov, B. Zhang, Y. Zhang and J. Wang, Graphene encapsulated FexCoy nanocages derived from metal–organic frameworks as efficient activators for peroxymonosulfate, *Catal. Sci. Technol.*, 2016, **6**(20), 7486–7494.
46 X. C. Feng, Z. J. Xiao, H. T. Shi, B. Q. Zhou, Y. M. Wang, H. Z. Chi, X. H. Kou and N. Q. Ren, How Nitrogen and Sulfur Doping Modified Material Structure, Transformed Oxidation Pathways, and Improved Degradation Performance in Peroxymonosulfate Activation, *Environ. Sci. Technol.*, 2022, **56**(19), 14048–14058.

 